Environ. Sci. Technol. **2005**, *39*, 7287−7293

Field Studies on the Formation of Sinking CO_2 Particles for Ocean Carbon Sequestration: Effects of Injector Geometry on Particle Density and Dissolution Rate and Model Simulation of Plume Behavior

DAVID E. RIESTENBERG,[†]
COSTAS TSOURIS,[*,†]
PETER G. BREWER,[*,‡]
EDWARD T. PELTZER,[‡] PETER WALZ,[‡]
AARON C. CHOW,[§] AND
E. ERIC ADAMS[*,§]

Oak Ridge National Laboratory, Post Office Box 2008, Oak Ridge, Tennessee 37831, Monterey Bay Aquarium Research Institute, 7700 Sandholdt Road, Moss Landing, California 95039-9644, and Department of Civil and Environmental Engineering, Massachusetts Institute of Technology, 77 Massachusetts Avenue, Cambridge, Massachusetts 02139

We have carried out the second phase of field studies to determine the effectiveness of a coflow injector which mixes liquid CO_2 and ambient seawater to produce a hydrate slurry as a possible CO_2 delivery method for ocean carbon sequestration. The experiments were carried out at ocean depths of 1000−1300 m in Monterey Bay, CA, using a larger injector than that initially employed under remotely operated vehicle control and imaging of the product. Solidlike composite particles comprised of water, solid CO_2 hydrate, and liquid CO_2 were produced in both studies. In the recent injections, the particles consistently sank at rates of ∼5 cm s^{-1}. The density of the sinking particles suggested that ∼40% of the injected CO_2 was converted to hydrate, while image analysis of the particle shrinking rate indicated a CO_2 dissolution rate of 0.76−1.29 μmol cm^{-2} s^{-1}. Plume modeling of the hydrate composite particles suggests that while discrete particles may sink 10−70 m, injections with CO_2 mass fluxes of 1−1000 kg s^{-1} would result in sinking plumes 120−1000 m below the injection point.

Introduction

The concept of ocean storage of anthropogenic CO_2 (*1*) at intermediate depths has been studied both in modeling (*2*−*4*) and laboratory settings (*5*−*7*) and through a series of small-scale oceanic injection experiments (*8*−*12*). No large-scale oceanic experiments have yet been carried out, and thus the extension of small-scale results requires models to predict the behavior of larger plumes. The incompressibility of seawater, combined with the high compressibility of liquid CO_2, typically results in a density reversal so that liquid CO_2 is buoyant at depths <2700 m and sinks at depths >3000 m. Because a strong correlation exists between depth of injection and oceanic retention time, an important design goal is to achieve deep injection while minimizing cost. As part of this effort, we examine the forcing of solid hydrate formation as a tool to generate a sinking mass of CO_2 at depths far less than those that can be accomplished by simple liquid injection into the ocean water column.

Modeling results of the behavior of large plumes composed of negatively buoyant or even neutrally buoyant CO_2 hydrate particles suggest that a sinking plume would result from the negative buoyancy of CO_2-rich water surrounding the dissolving particles (*13*−*14*). However, the production of particles with maximum negative buoyancy is clearly desirable in order to maximize the effective depth of disposal.

A method for producing sinking CO_2 particles has been developed (*7*, *13*) in which CO_2 and water are mixed at intermediate ocean pressures and temperatures by coflow injection of seawater and liquid CO_2. Hydrate shells form on the fluid/fluid interface, creating a solidlike composite consisting of unconverted liquid CO_2, water, CO_2 hydrate, and rejected brine which is extruded from the injector tip into the seawater. The degree of conversion of CO_2 to its hydrate form determines the density of the composite and, therefore, the depth at which sinking particles may be produced (*15*).

Recently, we reported the first results of field studies on the injection of such a composite at 1100−1300-m ocean depth in Monterey Bay, CA (*11*). Ambient seawater was pumped through a 254-μm i.d. capillary tube at a flow rate of 50 mL/min into a 6.4-mm outer tube through which a stream of CO_2 was injected at flow rates of 10−50 mL/min. In these experiments, the production of composite particles varying from floating to slightly sinking was demonstrated. Particles were followed vertically by the remotely operated vehicle (ROV) and were imaged with high-definition television for some time after injection. Calculations based on the sinking velocity of the particles suggested that 20−30% of the CO_2 was converted to hydrate.

Hydrate formation is rapid at the interface between CO_2 and water. However, after the hydrate layer has encased the water droplets, formation slows considerably due to separation of the reactants by the hydrate film (*13*). Maximizing the surface area between the water and liquid CO_2 phases is the best way to form large amounts of hydrate and, therefore, sinking composite particles. Laboratory experiments were performed on the behavior of water jets injected into CO_2 and vice versa (*16*). It was observed that the smallest droplets of water, and therefore the highest interfacial area, in continuously flowing CO_2 were produced at injection flow rates sufficiently high that the water jet breakup occurs in "spray" mode. Water jet breakup patterns were also noted to fit the relationship established by Tang et al. (*17*). The spray mode occurs when the jet Weber number $W_e = \rho U^2 d_0 \sigma^{-1} > 320$, where ρ and U are the density and injection velocity of the injected liquid, respectively; σ is the surface tension; and d_0 is the capillary diameter. Using this relationship, it is possible to predict which flow rates will result in "spray" breakup for a given injector capillary diameter.

* Address corrresponence to either author. Phone: (865)241-3246 (C.T.); (831)775-1706 (P.G.B.); (617)253-6595 (E.E.A.). E-mail: tsourisc@ornl.gov (C.T.); brpe@mbari.org (P.G.B.); eeadams@MIT.EDU (E.E.A.).

† Oak Ridge National Laboratory, Post Office Box 2008, Oak Ridge, Tennessee 37831.

‡ Monterey Bay Aquarium Research Institute, 7700 Sandholdt Road, Moss Landing, California 95039-9644.

§ Department of Civil and Environmental Engineering, Massachusetts Institute of Technology, 77 Massachusetts Avenue, Cambridge, Massachusetts 02139.

10.1021/es050125+ CCC: $30.25 © 2005 American Chemical Society
Published on Web 08/06/2005

In designing a new coflow injector for the recent field injections, the focus was on two areas. First, higher CO_2 and water flow rates were available for these injections, so a larger water capillary was chosen. Flow rates of up to 140 mL/min were available from pumps on the Monterey Bay Aquarium Research Institute ROV *Ventana*. A capillary with a 50% greater internal diameter was chosen because it was predicted to produce a water "spray" jet breakup into the CO_2 stream at high flow rates (*16*). This allowed use of a larger-diameter CO_2 delivery line (the outer injector tube), and the combined flow resulted in a longer residence time of the composite inside the injector, thus creating a longer period for hydrate formation in the reactor extension. A larger CO_2 tube was also expected to decrease any injector-wall effects on water droplet formation and to prevent water droplet coalescence.

Methods and Materials

The coflow jet reactor used for the hydrate composite has been described in detail previously (*7*, *13*). Water is injected at high velocity through a capillary tube into a slower-moving stream of liquid CO_2 flowing through an outer tube. Because the two fluids are immiscible, the water jet breaks up into droplets that are then covered with CO_2 hydrate. The presence of hydrate stabilizes the droplets with respect to coalescence. Instead of coalescing, the droplets are fused together by hydrate, creating rod-shaped composite particles which have the diameter of the injector. These composite particles consist of hydrate-covered water droplets and unconverted CO_2 and break off periodically at weak points after passing the injector tip. For the injection experiments reported here, the i.d. for the water capillary used was 381 μm and that for the CO_2 delivery tube was 9.5 mm.

This larger coflow jet reactor was field tested in ocean waters from 900- to 1200-m depth in Monterey Bay, CA, in waters of 3.3−3.9 °C. The ROV *Ventana* was deployed by the RV *Point Lobos* to perform the injections. The procedure for the injection and particle analysis is similar to that used in the previous field injection studies (*11*). Briefly, the injector was mounted in an acrylic box that was open at the top and bottom and had an illuminated translucent rear panel (Figure 1). Baffles were added to the top and bottom of the box to achieve more uniform flow of the water as the vehicle transited the water column. The box allowed the injected composite particles to rise or fall freely based on their buoyancy but restricted lateral motion (*18*), thus easing the vehicle piloting requirements. Carbon dioxide and ambient seawater were pumped via piston assemblies (*8*). Volumetric flowmeters were installed to measure the flow rates of the fluids as they were introduced into the coflow jet reactor and were arranged so that they could be viewed via the primary HDTV camera system (*18*).

Injections were performed using water flow rates of 140−150 mL/min and CO_2 flow rates of 26−40 mL/min. This water flow rate was expected to produce a "spray"-type jet breakup in the liquid CO_2 (*16*), and this ratio of CO_2:H_2O has been demonstrated to produce sinking composite in the laboratory and the field (*11*, *13*). Video images were processed post-cruise, using image analysis software (*Adobe PhotoShop*) to determine the dimensions of the particle. Scales on the front and rear planes of the acrylic imaging box were used to measure the length and diameter of the cylindrical composite particles. The seawater depth, temperature, and pressure were logged throughout the experiment using the instrumentation suite installed on the ROV. These data were then used to estimate the velocity, density, and dissolution rate of each particle.

Results and Discussion

Sinking composite particles were successfully produced at depths of 1000−1200 m. Three rodlike extruded particles that were produced at 1200 m were followed by the ROV for 2−10 min as they sank in the acrylic box. One particle was formed at 1000 m and was followed as it sank for 7 min. Particles were observed until they became too small to be visualized by the camera, broke up into small pieces, or escaped from the top or bottom of the box due to turbulence. An image of a large particle produced at 1200 m and sinking freely in the box is provided in Figure 1. A summary of the injection flow rates, average particle sinking rates, and particle dimensions observed is provided in Table 1.

The particles produced by the larger injector used in these experiments all sank after injection. Figure 2 shows the vertical paths of the composite particles. Also shown in the figure are the paths of three particles that were followed in the field injection experiments that were conducted in 2002 using a smaller injector (*11*). The particles in this study sank at rates of 4.8−5.8 cm s^{-1}, and these rates appear to be consistent over the entire length of time that the particles were followed (Figure 2). Injections were also performed at 900 m and 4.3 °C. However, the hydrate composite produced was not cohesive and broke up into many small, wispy pieces immediately after injection. This observation may indicate that the critical P/T conditions required for successful

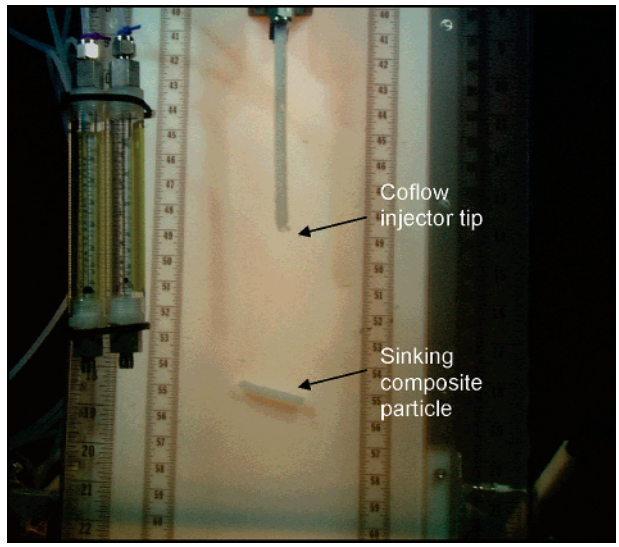

FIGURE 1. Injection of CO_2 hydrate composite at 1200 m, 3.3 °C. The tape measures used for image size analysis were glued to both the front and back of the box to correct for distance from the camera. The two flowmeters (upper left), which indicated both water and CO_2 flow rates in real time, were controlled by rotation of a needle valve (lower right) with the vehicle robotic arm. The vehicle was piloted so as to keep the extruded material inside the imaged space as it sank. Temperature and pressure (depth) were recorded continuously.

TABLE 1. Data for the Four Particles Followed by the ROV after Injection at 1200 m and 1000 m

	particle[a]			
	1200 m A	1200 m B	1200 m C	1000 m A
water flow rate (mL min^{-1})	140	140	140	150
CO_2 flow rate (mL min^{-1})	26	36	26	32
elapsed time (min)	10:17	3:44	2:01	7:36
sinking rate (cm s^{-1})	5.8	5.2	4.8	5.2
initial/final diameter (mm)	7.9/5.2	7.2/5.4	7.4/6.2	7.9/4.5
initial/final length (mm)	65.4/59.0	113.2/74.5	141.7[b]	70.4/57.8

[a] Particles "1200 m A", "1200 m B", and "1200 m C" were injected at a depth of 1200 m, temperature of 3.3 °C, and salinity of 34.6 ppt. Particle "1000 m A" was injected at a depth of 1000 m, temperature of 3.9 °C, and salinity of 34.5 ppt. [b] Final particle length measurement could not be obtained.

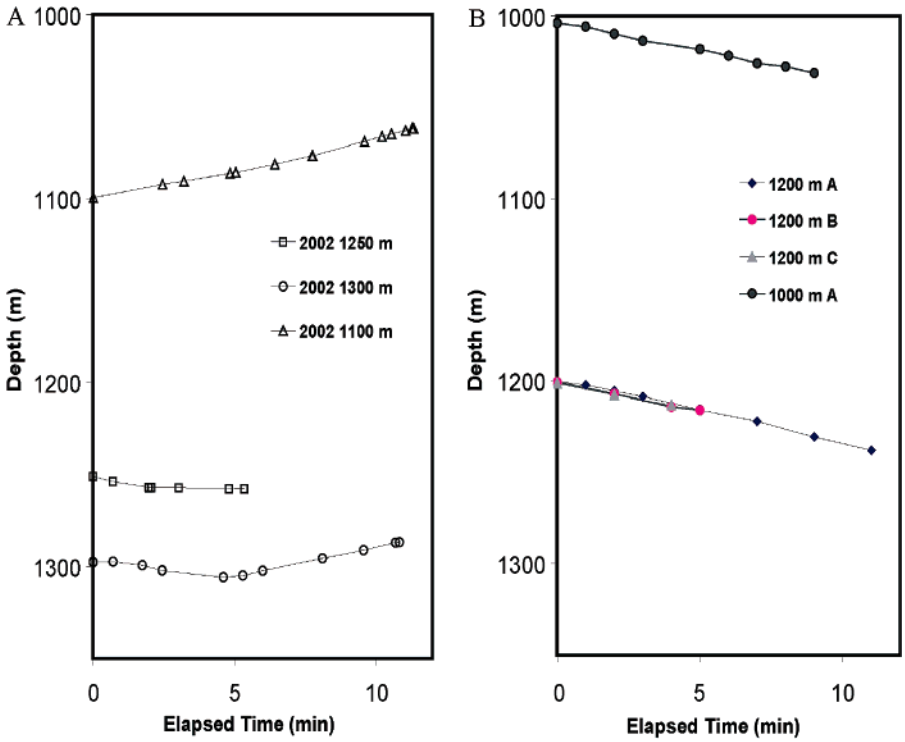

FIGURE 2. (A) Vertical paths of composite particles in 2002 injections. (B) Vertical paths of composite particles in 2004. Particles produced in the 2004 injections sank more rapidly and consistently than the particles produced in 2002.

cohesive composite particle formation were not achieved at this shallower and/or warmer depth.

Comparison with Past Field Injections. In Figure 2, the vertical positions of the composite particles from these injections, as well as those in the previous set of experiments, are plotted (*11*). It is apparent that the particles produced by the larger injector produced denser particles that consistently sank at a higher rate than those produced by the small injector. The density of the composite particles formed can be estimated by the method used in the previous study (*11*, *19*) using eq 1,

$$\rho_p = \rho_w + i\frac{3C_D\rho_w U_p^2}{4D_{ps}g} \tag{1}$$

where C_D is the drag coefficient; ρ_w is the density of seawater at the injection depth; U_p is the vertical velocity of the particle; i is +1 for a sinking particle and −1 for a floating particle; g is the gravitational constant; and D_{ps} is the diameter of the equivalent spherical particle $(1.5D_{pc}^2L_p)^{1/3}$, where L_p is the particle length and D_{pc} is the diameter of the actual cylindrical-shaped particle. The method to estimate the conversion of CO_2 to hydrate (x_h) based on a balance between particle negative buoyancy and drag has been described in detail previously (*11*). However, as described subsequently, several of the parameter values have been updated. The length, diameter, and velocity for each particle immediately after release from the injector were used to calculate the particle densities. A summary of particle data is presented in Table 2.

It should be noted that values for hydrate conversion (x_h) are very sensitive to uncertainties in several variables, such as the particle drag coefficient (C_D), the density of pure CO_2 hydrate (ρ_h), and the volume ratio of CO_2 to water that is actually incorporated into the composite (λ). The effects of these individual uncertainties are shown in Table 3 for changes in the calculated CO_2 conversion rate (x_h) for particle "1200 m A". In general, C_D depends on *Re* and particle shape. In the range of *Re* (computed using D_{ps}) observed for hydrate composite particles in the field, C_D for a sphere ranges from 0.49 to 0.83 (value of 0.49 for particle "1200 m A"; average of 0.60). Wadell (*23*) characterized C_D for nonspherical isometric particles as a function of particle sphericity ψ = area of a sphere of equivalent volume/area of particle. Wadell's values of C_D for the particles in Table 2 range from 1.42 to 4.28 (value of 4.28 for particle "1200 m A"; average of 3.4). Although Wadell's drag curves are widely used, data suggest significant dependence on particle shape for a given ψ. Isaacs and Thodos (*24*) observed the sinking of smooth cylinders of finite length; in terms of D_{ps}, their drag coefficient is

$$C_D = 0.96\gamma^{-0.12}\left(\frac{L_p}{D_{pc}}\right)^{0.25} \tag{2}$$

where $\gamma = (\rho_p/\rho_w)$ is the value of the specific gravity. For the particles of interest, γ raised to the low power is close to 1, so C_D is mainly a function of the cylinder aspect ratio. Using data in Table 2, eq 2 gives C_D ranging from 1.41 to 1.66 (value of 1.66 for particle "1200 mA"; average of 1.5), significantly lower than Wadell's predictions.

To investigate which drag coefficient model to apply for the hydrate composite particles in the field, laboratory experiments were conducted in a tall, wide glass tank (1.2 × 1.2 × 2.4 m) with particles made of extruded mixtures of cake frosting and shortening at room temperature. The mixtures were negatively buoyant, with measured densities and dimensions close to the hydrate particles in the field, and, like the hydrate composites, were roughly cylindrical when extruded from the nozzle. Descent velocities were measured by digitally filming individual particles, and plotting their vertical position versus time. Using eq 1, we obtained $C_D = 1.8 \pm 0.3$. Much of the variability is due to imprecision of our calculated densities, which are close to one, but we ascribe a portion to actual variability among particles, caused by asymmetrical extrusion, nonhomogeneous composition, etc. Isaacs and Thodos (*24*) noted that vortex shedding caused the particles to translate (sway) and rotate (pitch and yaw) during their descent. Our particles were also observed to

TABLE 2. Density and Dissolution Rates for Selected Particles from the 2004 and 2002 CO_2 Hydrate Composite Particle Injections

	2004 injections		2002 injections		
	1200 m A	1000 m A	163_1107	164_1226	164_1232
depth (m)	1200	1000	1099	1251	1297
temperature (°C)	3.3	3.9	3.6	3.3	3.2
H_2O flow, Q_w (mL min^{-1})	140	150	50	50	50
CO_2 flow, Q_c (mL min^{-1})	26	32	50	10	10
injector i.d. (mm)	381	381	254	254	254
est CO_2 density (g cm^{-3})[a]	0.97	0.955	0.963	0.973	0.9776
est water density (g cm^{-3})	1.033	1.032	1.033	1.033	1.034
salinity (ppt)	34.59	34.53	34.49	34.51	34.53
behavior	sink	sink	float	sink	neutral
sink rate (cm/s)	5.8	5.2	−6	2	0
particle density (g cm^{-3})	1.05	1.05	1.00	1.04	1.03
CO_2 conv (x_h)[a]	0.41	0.39	<0	0.20	0.16
shrink rate (mm s^{-1})[b]	4.36	6.64	5.30	7.40	4.10
particle diameter (cm)	0.79	0.79	0.60	0.60	0.57
particle length (cm)	7	6.5	2.46	3.4	2.62
D_{ps} (cm)	1.87	1.83	1.10	1.24	1.08
particle vol (cm^3)	3.43	3.19	0.70	0.99	0.67
CO_2 mass fraction	0.22	0.25	0.48	0.22	0.21
CO_2 DR (mmol cm^{-2} s^{-1})	0.76	1.29	2.97	1.38	0.76

[a] Densities for CO_2 were calculated using predictions for the ambient injection pressures (ocean depths) and temperatures using the latest NIST Webook data (*20*) and differ slightly from those used in Tsouris et al. (*11*). The value used for CO_2 hydrate density was 1.143 g cm^{-3} (*21*). [b] Shrinkage rates are for particle diameters.

TABLE 3. Uncertainties on the Calculations of Liquid CO_2 Conversion into Hydrate for Particle 1200 m A

variables	values	hydrate conversion (x_h)
particle drag coefficient (C_D)	0.49	0.24
	1.66[a]	0.41
	4.28	0.78
CO_2 hydrate density (g/cm^3)	1.143 [a,b]	0.41
	1.12[c]	0.49
	1.10[d]	0.60
CO_2/H_2O in particle (λ)	0.19	0.55
	0.34[a]	0.41
	0.46	0.36

[a] Values used for Table 2 calculations (particle 1200 mA) and Table 3 calculations (base case). [b] Hydrate density from ref 21. [c] Hydrate density from ref 4. [d] Hydrate density from ref 22.

wobble during their descent, with the magnitude of wobbling varying among particles. We suspect that similar variability could occur in the hydrate composite particles. Table 3 indicates that by using a conservative value, based on eq 2, of $C_D = 1.5$, the predicted conversion is about 50% for particle "1200 m A". The lowest possible particle density would be obtained by treating it as a sinking sphere, giving a minimum conversion of 28%, while using C_D based on Wadell's sphericity would overestimate the particle density, resulting in a conversion of 78%. Equation 2 provided values of C_D close to those observed in the lab, and is thus used to estimate the particle densities in Tables 2 and 3.

In addition, due to the similarity in densities among all three of the composite components, using different reported densities for CO_2 hydrate was also found to affect x_h significantly, with higher densities giving lower x_h values. Finally, laboratory observations suggest that some of the unreacted water was excluded from the composite, resulting in an increase of λ and a corresponding decrease in x_h for sinking particles (Table 3). For example, if particle "1200 m A" incorporated all of the unreacted water plus CO_2 into the composite, the value of λ (based on the respective flow rates entering the reactor) would be 0.19. Conversely the value of λ for the stoichiometric hydration of all of the CO_2 is 0.46. Our estimate for λ in Table 2, and the base case for Table 3, is the average of the above two extremes.

CO_2 Dissolution Rates. Image analysis was conducted on selected particles in order to calculate their shrinkage rate as well as to derive a CO_2 dissolution rate. As with previous experiments, particle length and width measurements were made on selected video frames in which the particles appeared to be aligned parallel to the front of the acrylic box. Shrinkage rates for particle diameters are presented in Figure 3. The particle diameters shrank at rates from 4.4 to 10.6 μm s^{-1}. Rehder et al. (*25*) investigated the shrinkage and dissolution of pure cylindrical specimens of CO_2 and methane hydrate in samples held in cages near the ocean floor at 1028 m. They reported diameter shrinkage rates for their CO_2 hydrate samples of 0.94 and 1.20 μm s^{-1}.

Given the particle diameter shrinkage rate observed and the mass fraction of CO_2 input in the coflow injection determined from the flowmeter data, a CO_2 dissolution rate (*DR*) for our experiments can be calculated using eq 3,

$$DR = \frac{1}{2}\left(\frac{dD_p}{dt}\right)\rho_p \frac{\varphi}{MW_{CO2}} \tag{3}$$

where D_p is the particle diameter; ρ_p is the composite density; and MW_{CO_2} is the molecular weight of CO_2 (44 g mol^{-1}). The mass fraction of CO_2 in the composite, φ, is equivalent to

$$\varphi = \frac{Q_c\rho_c}{Q_c\rho_c + Q_w\rho_w} \tag{4}$$

where Q_c and Q_w are the CO_2 and water injection flow rates, respectively; and ρ_c and ρ_w are the CO_2 and water densities at the injection depths, respectively. Here we must assume that 100% of both fluids is made into composite with none escaping prior to dissolution.

Dissolution rates were calculated using eq 3 for a particle at each depth that was tracked for the longest period of time (particles "1200 m A" and "1000 m A"). Calculated dissolution rates were 0.76 and 1.29 μmol CO_2 cm^{-2} s^{-1}, respectively. Dissolution rates calculated for the particles from the 2002 injections are also presented in Table 2. Rehder et al. (*25*) report dissolution rates of 0.36-0.46 μmol CO_2 cm^{-2} s^{-1} for stationary solid pieces of CO_2 hydrate held near the seafloor at 1028 m, while Brewer et al. (*18*) reported a dissolution rate of 3.0 μmol CO_2 cm^{-2} s^{-1} for hydrate-covered CO_2 droplets

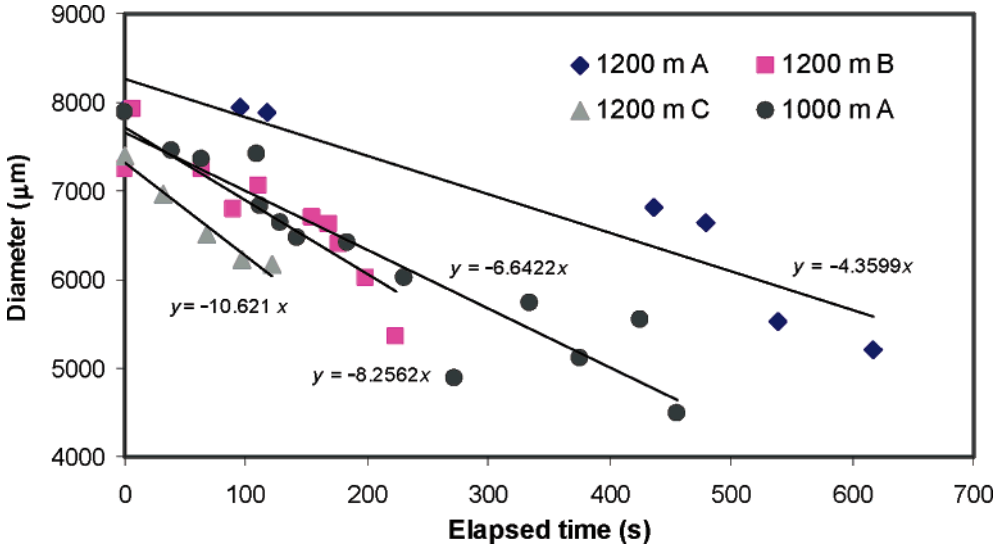

FIGURE 3. Composite particle diameter shrinkage rates after injection in 2004 (μm s^{-1}).

released at 800 m and rising at a rate of 10 cm/ s. It seems reasonable that the composite particles in this study would have dissolution rates between that of stationary pure CO_2 hydrate and that of rising hydrate-covered CO_2 droplets since the composite produced in these injections contained >70% unconverted CO_2 and sank at a rate of about 5 cm/s. This correspondence with earlier work gives us confidence in the results reported here.

Extrapolation to Field-Scale Plumes. Three of the 5 composite particles identified in Table 2 were observed to sink as a result of their negative buoyancy. However, significantly greater sinking would occur if a large number of such particles were released as a continuous stream. There are two reasons for the expected increase in sinking. First, a continuous stream of negatively buoyant particles creates a negatively buoyant plume that entrains ambient seawater, resulting in significantly larger vertical velocities (seawater plus sinking particles), and hence effective depths of disposal (*14*, *26*, *27*). Second, the dissolving CO_2 increases the density of the seawater, causing further descent, and decreases (slightly) the dissolution rate, thus extending the lifetime of the solid. Wannamaker and Adams (*14*, *27*) predict that plumes of negatively buoyant, spherical, *pure* CO_2 hydrate particles that are released into quiescent receiving water will sink up to 8 times deeper than would the particles individually, with the greatest "plume effect" occurring for the smallest particles and the largest CO_2 loadings. Analogous efficiency should accrue for plumes composed of particles of partially reacted CO_2.

To explore this matter quantitatively, we have modified the integral double plume model of Wannamaker and Adams (*14*, *27*) to apply to cylindrical composite particles. The model expresses the composition of the particles in terms of the mass ratio of seawater to carbon dioxide and the fraction of the carbon dioxide converted to hydrate. The cylindrical particles shrink at the same rate as observed in Table 2 (neglecting the small decrease in dissolution rate expected due to the increased concentration of CO_2 in the plume water) and retain the same composition until they are completely dissolved. The dissociation of CO_2 and its effect on the pH and density of the surrounding plume fluid are modeled as if they are instantaneous. It is recognized that complete carbonate system equilibrium includes the relatively slow hydration reaction, which has a relaxation time of about 4 min at water temperatures of 3−4 °C (*28*, *29*); however this is still significantly faster than the time scale of 20−30 min for particle dissolution.

TABLE 4. Depth of Sinking (in Meters) for Discrete Particle and Plumes with a Continuous Stream of Particles

	composite particle		
	1200 m A	1000 m A	164_1226
discrete particle	69	41	10
particle plume			
CO_2 mass flux = 1 kg s^{-1}	169	126	123
CO_2 mass flux = 10 kg s^{-1}	303	229	223
CO_2 mass flux = 100 kg s^{-1}	540	496	486
CO_2 mass flux = 1000 kg s^{-1}	1074	979	961

The fall velocities of both the individual particles and the particles contained within a plume are calculated as a function of the Reynolds number (based on the diameter of an equivalent spherical particle) and the particle density such that their initial velocities match those given in Table 2. As mentioned earlier, nonspherical particles may have significantly higher drag coefficients than the equivalent sphere (*19*), but this would be manifest in higher calculated particle densities, resulting in the same slip velocity. The higher particle densities would not significantly affect the depth of descent of individual particles, but would cause particle *plumes* to sink somewhat further, making our calculations conservative.

Table 4 shows the calculated maximum depths of descent for plumes composed of the three negatively buoyant particles that were observed, assuming initial CO_2 mass fluxes of 1, 10, 100, and 1000 kg/s. For reference, a 500-MW coal plant will produce a CO_2 stream of approximately 123 kg/s (*30*). Also indicated are the calculated depths of descent for the individual particles. Table 5 shows the associated increase in concentration of dissolved inorganic carbon and the decrease in pH of the plume water for each of the plume calculations. Clearly, the depth of sinking increases with CO_2 flow rate and greatly exceeds the level that would be achieved by individual composite particles. Of course, concentration and pH perturbations also increase with increasing CO_2 flow rate, and an optimal rate might be found that balances depth of sequestration with concentration and pH perturbation.

Figure 4 depicts model output for one release condition (100 kg/s of CO_2 in the form of particles with the characteristics of particle "1200 m A"). The rate at which the CO_2 that dissolves from individual particles enters the water column is proportional to the diameter shrinkage rate (presumed constant) times the diameter squared; hence,

TABLE 5. Increase in Dissolved Inorganic Carbon Concentration (in Kilograms per Cubic Meter) and Decrease in pH (in Parentheses) for Plumes with a Continuous Stream of Particles

	composite particle		
	1200 m A	1000 m A	164_1226
particle plume			
CO_2 mass flux = 1 kg s^{-1}	0.04 (1.0)	0.07 (1.2)	0.07 (1.2)
CO_2 mass flux = 10 kg s^{-1}	0.07 (1.2)	0.11 (1.5)	0.11 (1.5)
CO_2 mass flux = 100 kg s^{-1}	0.12 (1.5)	0.15 (1.6)	0.15 (1.6)
CO_2 mass flux = 1000 kg s^{-1}	0.18 (1.7)	0.21 (1.7)	0.22 (1.7)

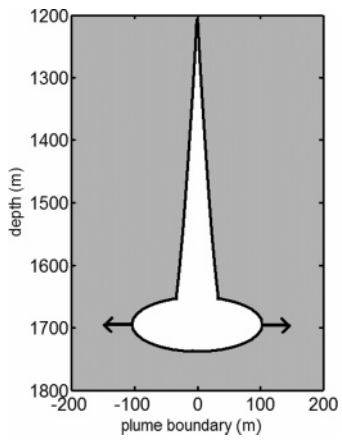

FIGURE 4. Sketch of the sinking plume resulting from a simulated release of 100 kg s^{-1} of CO_2 in the form of cylindrical hydrate composite particles with the characteristics of particle "1200 m A" (described in Table 2).

most of the CO_2 will dissolve during the upper part of the particle's descent. By contrast, the dissolved CO_2 that intrudes into the ambient water column as the result of a plume will be concentrated near the maximum depth of descent.

These results pertain to discharge into quiescent seawater. In a strong ambient current, the difference between plume sinking and individual particle sinking would be less than that implied in Table 4 because a strong current causes the dispersed phase to separate from the plume (*31*). On the other hand, the difference could be greater than indicated if the individual particles break into smaller (slower-settling) particles before they dissolve completely (as was observed in the field).

With our current injector system, the plume shown in Figure 4 (corresponding to a typical power plant) would require loading of about 10^5 particles per second. Clearly some changes to the injection system would be required in scaling up to such release rates. While details are beyond the scope of this paper, the scale-up might involve one or more of the following approaches. First, the size of the injector (i.e., the capillary tube delivering the water) and the reactor itself could be increased, forming larger composite particles. Second, the number of injectors per reactor injector could be increased. Third, a number of such reactors could contribute to a plume. Finally, multiple injection plumes could be employed for each power plant.

Implications for Future Research. The sinking behavior of composite particles alone is a desirable property because it carries CO_2 to deeper waters, which should lead to longer sequestration. Additional study is required to better quantify composite density and hence composition. As particles descend, a relatively slow dissolution occurs, which is additionally desirable for two reasons. First, it disperses CO_2 in the water column, so that local concentrations of CO_2 are kept low. Second, as particles dissolve, the surrounding water becomes denser, forming a sinking plume. Simulations have shown that plumes containing particles similar to those generated in field experiments sink an order of magnitude deeper than discrete particles. This is a remarkable finding that needs to be verified in field experiments. Furthermore, the generation of sinking CO_2 particles via specially designed injectors may lead to a safer, longer-term, and less expensive way to sequester CO_2 in the ocean. However, before this technique can be applied on a large scale, further experimental and simulation studies are needed to investigate scale-up issues related to the injector geometry and flowrates and whether multiple injectors and/or injection points will be needed for a single power plant.

Acknowledgments

Gratefully acknowledged is support by the Ocean Carbon Sequestration Program, Office of Biological and Environmental Research, U.S. Department of Energy, Grant KP1202030, under Contract DE-AC05-00OR22725 with UT-Battelle, LLC and Contract DE-FG02-01ER63078 with MIT. Support for MBARI was provided by the David and Lucille Packard Foundation and the U.S. Department of Energy under Contracts DE-FC26-00NT40929 and DE-FG03-01-ER63065. We thank the captain and crew of the RV *Point Lobos* and the pilots of the ROV *Ventana* for their excellent work in making the field experiments possible. We also thank Dr. Marsha Savage for editing the manuscript.

Literature Cited

(1) Marchetti, C. On geoengineering the CO_2 problem. *Clim. Change* **1977**, *1*, 59−68.
(2) Haugan, P. M.; Drange, H. Sequestration of CO_2 in the deep ocean by shallow injection. *Nature* **1992**, *357*, 318−320.
(3) Liro, C. R.; Adams, E. E.; Herzog, H. J. Modeling the release of CO_2 in the deep ocean. *Energy Convers. Manage.* **1992**, *33*, 667−674.
(4) Holder, G. D.; Cugini, A. V.; Warzinski, R. P. Modeling clathrate hydrate formation during carbon-dioxide injection into the ocean. *Environ. Sci. Technol.* **1995**, *29*, 276−278.
(5) Teng, H.; Yamasaki, A. Dissolution of buoyant CO_2 drops in a counterflow water tunnel simulating the deep ocean waters. *Energy Convers. Manage.* **2000**, *41*, 929−937.
(6) Yamasaki, A.; Wakatsuki, M.; Teng, H.; Yanagisawa, Y.; Yamada, K. A new ocean disposal scenario for anthropogenic CO_2: CO_2 hydrate formation in a submerged crystallizer and its disposal. *Energy* **2000**, *25*, 85−96.
(7) West, O. R.; Tsouris, C.; Liang, L.; Lee, S. Y.; McCallum, S. D. Negatively buoyant CO_2-hydrate composite for ocean carbon sequestration. *AIChE J.* **2003**, *49*, 283−285.
(8) Brewer, P. G.; Orr, F. M., Jr.; Friederich, G.; Kvenvolden, K. A.; Orange. D. L. Gas hydrate formation in the deep sea: In situ experiments with controlled release of methane, natural gas, and carbon dioxide. *Energy Fuels* **1998**, *12*, 183−188.
(9) Brewer, P. G.; Friederich, G.; Peltzer, E. T.; Orr, F. M., Jr. Direct experiments on the ocean disposal of fossil fuel CO_2. *Science* **1999**, *284*, 943−945.
(10) Brewer, P. G.; Peltzer, E. T.; Aya, I.; Haugan, P.; Bellerby, R.; Yamane, K.; Kojima, R.; Walz, P.; Nakajima, Y. Small scale field study of an ocean CO_2 plume. *J. Oceanogr.* **2004**, *60*, 751−758.
(11) Tsouris, C.; Brewer, P. G.; Peltzer, E.; Walz, P.; Riestenberg, D.; Liang, L.; West, O. R. Hydrate composite particles for ocean carbon sequestration: Field verification. *Environ. Sci. Technol.* **2004**, *38*, 2470−2475.
(12) Aya, I.; Kojima, R.; Yamane, K.; Brewer, P. G.; Peltzer, E. T. In situ experiments of cold CO_2 release in mid-depth. *Energy* **2004**, *29*, 1499−1509.
(13) Lee, S.-Y.; Liang, L.; Riestenberg, D. E.; West, O. R.; Tsouris, C.; Adams, E. E. CO_2 hydrate composite for ocean carbon sequestration. *Environ. Sci. Technol.* **2003**, *37*, 3701−3708.
(14) Wannamaker, E. J.; Adams, E. E. Modeling descending carbon dioxide injections in the ocean. *Proc. 6th Int. Conf. Greenhouse Gas Control Technol.*, **2002**, 753−758.

(15) Gabitto, J.; Riestenberg, D. E.; Lee, S. Y.; Liang, L.; Tsouris, C. Ocean disposal of CO_2: Conditions for producing sinking CO_2 hydrate. *J. Dispersion Sci. Technol.* **2004**, *25*, 705−714.
(16) Riestenberg, D. E.; Chiu, E.; Gborigi, M.; Liang, L.; West, O. R.; Tsouris, C. Investigation of jet breakup and droplet size distribution of liquid CO_2 and water systems−implications for CO_2 hydrate formation for ocean carbon sequestration. *Am. Mineral.* **2004**, *89*, 1240−1246.
(17) Tang, L.; Gorgas, T. J.; Masutani, S. M. Liquid CO_2 droplet spectra. *Proc. 6th Int. Conf. Greenhouse Gas Control Technol.*, **2002**.
(18) Brewer, P. G.; Peltzer, E. T.; Friederich, G.; Rehder, G. Experimental determination of the fate of rising CO_2 droplets in seawater. *Environ. Sci. Technol.* **2002**, *36*, 5441−5446.
(19) Tek, M. R.; Wilkes, J. O. *Fluid Flow and Heat Transfer*; University of Michigan: Ann Arbor, 1974.
(20) *NIST Standard Reference Database 69, March 2003 Release, NIST Chemistry WebBook. http://webook.nist.gov/chemistry/* (accessed Nov. 2004).
(21) Circone, S.; Stern, L. A.; Kirby, S. H.; Durham, W. B.; Chakoumakos, B. C.; Rawn, C. J.; Rodinone, A. J. CO_2 hydrate: Synthesis, composition, structure, dissociation behavior, and a comparison to Structure I CH_4 hydrate. *J. Phys. Chem. B* **2003**, *107*, 5529−5539.
(22) Aya, I.; Yamane, K.; Nariai, H. Solubility of CO_2 and density of CO_2 hydrate at 30 MPa. *Energy* **1997**, *22*, 263−271.
(23) Wadell, H. The coefficient of resistance as a function of Reynolds number for solids of various shapes. *J. Franklin Inst.* **1934**, *217*, 459−490.
(24) Isaacs, J. L.; Thodos, G. The free-settling of solid cylindrical particles in the turbulent regime. *Can. J. Chem. Eng.* **1967**, *45*, 150−155.
(25) Rehder, G.; Kirby, S. H.; Durham, W. B.; Stern, L. A., Peltzer, E. T.; Pinkston, J.; Brewer, P. G. Dissolution rates of pure methane hydrate and carbon-dioxide hydrate in undersaturated seawater at 1000-m depth. *Geochim. Cosmochim. Acta* **2004**, *68*, 285−292.
(26) Asaeda, T.; Imberger, J. Structure of bubble plumes in linearly stratified environments. *J. Fluid Mech.* **1993**, *249*, 35−57.
(27) Wannamaker, E.; Adams, E. Modeling descending carbon dioxide injection in the ocean. *J. Hydraul. Res.*, in press.
(28) Johnson, K. S. Carbon-dioxide hydration and dehydration kinetics in seawater. *Limnol. Oceanogr.* **1982**, *27*, 849−855.
(29) Soli, A. L.; Byrne, R. H. CO_2 system hydration and dehydration kinetics and the equilibrium CO_2/H_2CO_3 ratio in aqueous NaCl solution. *Mar. Chem.* **2002**, *78*, 65−73.
(30) Herzog, H. J.; Golomb, D. S.; Zemba, S. Feasibility, modeling and economics of sequestering power-plant CO_2 emissions in the deep ocean. *Environ. Prog.* **1991**, *10*, 64−74.
(31) Socolofsky, S. A.; Adams, E. E. Multiphase plumes in uniform and stratified cross-flow. *J. Hydraul. Res.* **2002**, *4*, 661−672.

Received for review January 19, 2005. Revised manuscript received June 17, 2005. Accepted June 22, 2005.

ES050125+